Boundary-Element Shape Sensitivity Analysis for Thermal Problems with Nonlinear Boundary Conditions

James H. Kane* and Hua Wang†
Clarkson University, Potsdam, New York 13676

Implicit differentiation of the discretized boundary integral equations governing the conduction of heat in solid objects subjected to nonlinear boundary conditions is shown to generate an accurate and economical approach for the computation of shape sensitivities for this class of problems. This approach involves the employment of analytical derivatives of boundary-element kernel functions with respect to shape design variables. A formulation is presented that can consistently account for both temperature-dependent convection and radiation boundary conditions. Several iterative strategies are presented for the solution of the resulting sets of nonlinear equations and the computational performances examined in detail. Multizone analysis and zone condensation strategies are demonstrated to provide substantive computational economies in this process for models with either localized nonlinear boundary conditions or regions of geometric insensitivity to design variables. A series of nonlinear example problems are presented that have closed-form solutions.

Introduction

TEXTBOOK treatments[1-3] and technical articles[4-15] on boundary-element analysis (BEA) have shown it capable of predicting the thermal response of solids subjected to temperature-dependent boundary conditions. In Ref. 16, a zone condensation technique was shown to dramatically reduce the computer resources required to perform each of the linear steps involved in nonlinear thermal BEA, due to the ability to perform sparse blocked matrix factorizations of changing left-hand-side matrices of significantly reduced size. Articles concerned with the assembly and solution of unsymmetric, sparse blocked matrix equations associated with multizone BEA include those by Lachat and Watson,[17,19] Lachat,[18] Crotty,[20] and Das.[21] Bialecki and Nahlik[22] and Bialecki[23] describe an unsymmetric sparse blocked frontal equation-solving algorithm for solving BEA nonlinear heat transfer problems. Tomlin[24] and Butterfield and Tomlin[25] present similar treatments for nonhomogeneous continuum problems that are modeled as multiple piecewise homogeneous boundary-element zones. Beer,[26] Mustoe,[27] and Davies[28] describe procedures coupling boundary elements and finite elements in the same analysis and condense the BEA matrices to just the degrees of freedom on the boundary-element finite element interface. Condensation in BEA is also discussed by Jin et al.[29] and Margenov et al.[30] in conjunction with elastic contact problems. Kane,[31] Kane and Saigal,[32,36] Saigal and Kane,[33] and Saigal et al.[34,35] have shown that a multizone BEA and sensitivity analysis approach significantly impacts on the ability to exploit additional matrix sparsity present in the design sensitivity analysis step occurring during shape optimization of objects with partial geometric sensitivity. Kane and Saigal[37,38] have also used BEA zone condensation to obtain significant computational economies in structural shape optimization. Recently, Kane et al.[39] have shown how multizone capability can facilitate the effective utilization of reanalysis techniques in continuum structural shape optimization.

Design sensitivity analysis (DSA) refers to the process of computing rates of change of response quantities associated with an object with respect to changes in the parameters (design variables) that control its shape. These rates of change (sensitivities) are used in shape optimization by the numerical optimization procedure to determine effective search directions and move lengths in the space of the design variables. Economical and accurate DSA computation is a pacing item in the attempt to make larger-scale two-dimensional and fully three-dimensional shape optimization tractable. Implicit differentiation[32-36] of the discretized boundary integral equations has been shown to be an effective strategy for the formulation of DSA relations in linear heat transfer and stress analysis. The major advantage of this approach is that it obviates the requirement to factor perturbed left-hand-side matrices, but instead allows for the multiple reuse of the LU factorization of the current BEA system matrix formed during the last analysis. For thermal problems with nonlinear boundary conditions, including both temperature-dependent convection and radiation boundary conditions, the discretized boundary integral equations are nonlinear, and their solution is accomplished by iterative procedures. In this paper, implicit differentiation of these nonlinear equations is discussed. It is demonstrated that this approach can be used to generate a nonlinear DSA formulation that retains the positive beneficial characteristics present in linear DSA. Several iterative strategies are presented for the solution of the resulting sets of nonlinear DSA equations and the computational performances examined in detail. It is shown that the specific strategy used to solve the nonlinear equations during the thermal analysis has a major impact on the subsequent solution of the nonlinear equations associated with DSA. Multizone analysis and zone condensation strategies are also shown to provide substantive computational economies for models with either localized nonlinear boundary conditions or regions of geometric insensitivity to design variables. A series of nonlinear example problems are examined that have closed-form solu-

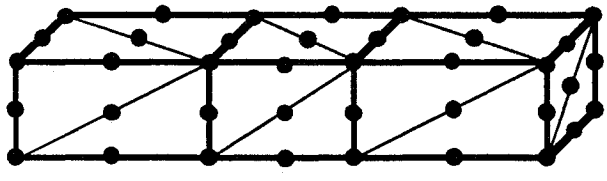

Fig. 1 Three-zone BEA model.

Received Nov. 20, 1989; revision received June 26, 1990; accepted for publication July 24, 1990.

*Associate Professor, Mechanical & Aeronautical Engineering Department.

†Graduate Research Assistant, Mechanical & Aeronautical Engineering Department.

tions. Exact analytical expressions for the shape sensitivities associated with these problems are compared with the sensitivities computed using the BEA formulation.

Nonlinear Boundary-Element Analysis Formulation

A two-dimensional thermal BEA formulation is discussed in Refs. 1–3. The resulting integral equation is

$$cT(d) + \sum_{E=1}^{NEL} \left\{ \int_{-1}^{+1} q^* \{H\} J \, da \right\}^{(E)} \{T\}^{(E)} = \sum_{E=1}^{NEL} \left\{ \int_{-1}^{+1} T^* \{H\} J \, da \right\}^{(E)} \{q\}^{(E)} \quad (1)$$

where T^* and q^* are the fundamental temperature and heat-flux solutions to the heat-conduction problem, $\{H\}$ is a row vector of element interpolation functions associated with each node on element E, a is an element intrinsic coordinate that runs from -1 to $+1$ in each element, and J is the Jacobian of the transformation from the actual coordinate system to the element's intrinsic coordinate system. $\{T\}^{(E)}$ and $\{q\}^{(E)}$ are column vectors of node point temperatures and normal heat-flux components, respectively, for element E and have been taken outside the integrals shown to produce an algebraic expression. A singular boundary-element formulation is obtained by locating the source point at each of the nodes present in the boundary-element model, producing a square system of algebraic equations.

$$[F]\{t\} = [G]\{q\} \quad (2)$$

where $\{t\}$ and $\{q\}$ are column vectors of nodal point temperatures and normal heat-flux components, respectively. The $\{t\}$ vector has an entry for each node in the overall problem, whereas the $\{q\}$ vector may have additional entries if jumps in the normal component of the heat flux occur at any node. The matrix $[F]$ is square, and $[G]$ is either square or rectangular.

In a well-posed boundary value problem, half of the temperature and normal heat-flux components will be specified and the other half will be unknown. By transferring all known values to the vector $\{q\}$, placing all unknown temperature and normal heat-flux components in the vector $\{t\}$, exchanging corresponding columns of the respective rectangular matrices, and performing the indicated matrix-vector multiplication on the right-hand side, a solvable system of equations can be produced

$$[A]\{x\} = \{b\} \quad (3)$$

Note that the notation has been generalized so that $\{t\}$ is the vector of unknown boundary response quantities, whereas $\{q\}$ denotes the vector of specified boundary conditions in the problem.

Convection boundary conditions relate the normal heat flux q on the surface of an object to the surface temperature T, the freestream (or bulk) temperature T_∞, and a convection coefficient h. By considering the ith equation in Eq. (2), substitution of the convection law for a convection boundary condition at node k yields

$$q = h(T - T_\infty) \quad (4)$$

$$\begin{aligned} f_{i1}T_1 + f_{i2}T_2 + \cdots + f_{ik}T_k + \cdots + f_{in}T_n &= g_{i1}q_1 + g_{i2}q_2 + \cdots + g_{ik}q_k + \cdots + g_{in}q_n \\ &= g_{i1}q_1 + g_{i2}q_2 + \cdots + g_{ik}h_k(T_k - T_\infty) + \cdots \\ &\quad + g_{in}q_n \end{aligned} \quad (5)$$

In Eq. (5), the temperature at node k appears on both the left- and right-hand side. Different approaches can be taken to solve these equations. One consists of leaving T_k on both sides and iterating to find its correct value, as

$$\begin{aligned} f_{i1}T_1 + f_{i2}T_2 + \cdots + f_{ik}T_k^{(j+1)} + \cdots + f_{in}T_n &= g_{i1}q_1 + g_{i2}q_2 + \cdots + g_{ik}h_k(T_k^{(j)} - T_\infty) + \cdots + g_{in}q_n \end{aligned} \quad (6)$$

In a second approach, the terms that multiply T_k on the right side of Eq. (5) are brought to the left.

$$\begin{aligned} f_{i1}T_1 + f_{i2}T_2 + \cdots + (f_{ik} - g_{ik}h_k)T_k + \cdots + f_{in}T_n &= g_{i1}q_1 + g_{i2}q_2 + \cdots + g_{ik}(-h_kT_\infty) + \cdots + g_{in}q_n \end{aligned} \quad (7)$$

For cases where h is not a function of T, the second method is preferred because it results in a linear problem. When h is a function of T, both approaches can be attempted, however, there are many cases in which the approach characterized by Eq. (6) does not converge. Other solution strategies have been presented[4–15] that are related to the Newton-Raphson iterative technique for the solution of simultaneous nonlinear equations, and they behave very similarly to the approach characterized in Eq. (7). In subsequent sections, it is shown that the choice of the solution strategy made here has significant impact on the effectiveness of the nonlinear DSA computations described in this paper.

The approach characterized by Eq. (6) leaves the left-hand side of the overall BEA system equations unchanged from one iteration to the next, thus allowing the triangular factorization of $[A]$, formed in the first iteration, to be reused in all subsequent iterations. The second method involves changing $[A]$ in each iteration. It has been shown[16] that algorithms that employ this left-hand-side modification strategy converge in just a few iterations, whereas algorithms that only modify the right-hand side of BEA system equations converge at a much slower rate and may actually diverge. It has also been shown[16] that BEA zone condensation techniques reduce the computational effort associated with the refactorization of partially modified left-hand-side matrices to the point where the overall algorithm becomes superior to other approaches for this class of problems.

The law for the normal heat flux on the surface of an object due to radiation can be manipulated into a form that makes it

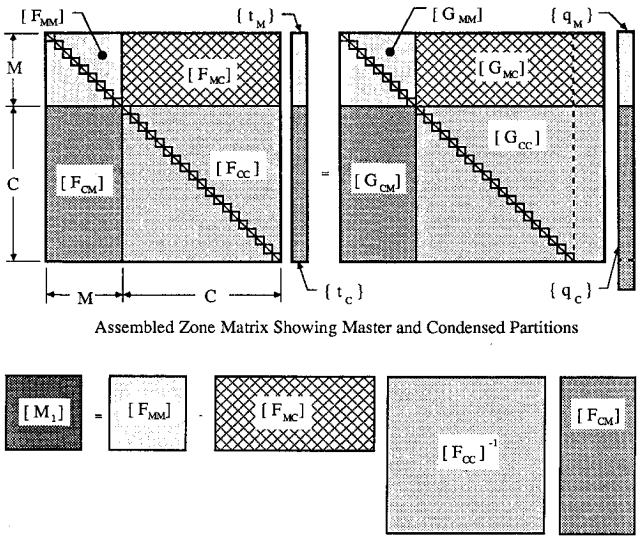

Fig. 2 Details associated with the assembly, reordering, partitioning, and condensation of boundary-element zone matrices.

appear exactly like a temperature-dependent convection coefficient

$$q = \sigma E(T^4 - T_r^4) \tag{8}$$

and

$$E = V\left\{\frac{1}{\epsilon} + \frac{1}{\epsilon_r} - 1\right\}^{-1}$$

$$q = \sigma E(T^2 + T_r^2)(T + T)(T - T_r) = h_r(T - T) \tag{9}$$

where σ is the Stefan-Boltzmann constant, T the surface temperature, T_r the temperature of the known external radiation source, V the radiation view factor, ϵ the surface emissivity of the object being analyzed, and ϵ_r the emissivity of the radiation source. It is therefore possible to solve problems involving radiation boundary conditions using a nonlinear BEA code that allows for a temperature-dependent convection coefficient that behaves like the cubic polynominal just presented.

Multizone Boundary Element Analysis

Multizone BEA[17-25] is accomplished by breaking up an entire model into zones as illustrated by the three-zone model shown in Fig. 1. The boundary integral relationship can be written for each zone and evaluated at node point locations for the zone in question to generate a matrix system.

$$[F^i]\{t^i\} = [G^i]\{q^i\} \tag{10}$$

In this equation, $[F^i]$ and $[G^i]$ are square and rectangular zone coefficient matrices, respectively, and $\{t^i\}$ and $\{q^i\}$ are column vectors of zone node point temperature and normal heat-flux components, respectively, of conformable size. In all symbols shown, the i superscript denotes that the superscripted quantities are those associated with the ith zone in a multizone BEA model. The matrix relations written for individual zones can be put together for use in an overall analysis by considering the temperature compatibility and thermal energy conservation of normal heat flux at zone interfaces.

$$\{t_{ij}^i\} = \{t_{ij}^j\}; \qquad \{q_{ij}^i\} = -\{q_{ij}^j\} \tag{11}$$

The negative sign must be present in the zone interface heat-flux relation to account for the opposite directions of the outward surface normals in the two zones in question. The double subscript notation is used to convey that the vector in question contains components entirely on the interface between zone i and zone j. By expanding the size of the zone matrix equations to the size of the overall problem, bringing the unknown heat fluxes at zone interfaces to the left side of the equation, and using the compatibility and conservation relations, the system equations for the overall multizone BEA problem can be formed. For example, the equations for the three-zone problem shown in Fig. 1 are given next. It should be noted that this model has no interface between zone 1 and zone 3. In this instance, the final multizone BEA system of equations can be produced by simply removing the blocks associated with this 1-3 interface shown in Eq. (12). Equation (2) can still be used to symbolize the overall sparse blocked hypermatrix equations characterized in more elaborate detail by Eq. (12).

$$\begin{bmatrix} [F_{11}^1] & [F_{12}^1] & [0] & -[G_{12}^1] & [0] & [0] & [0] & [0] & [0] \\ [0] & [F_{12}^2] & [0] & [G_{12}^2] & [F_{22}^2] & [F_{23}^2] & [0] & -[G_{23}^2] & [0] \\ [0] & [0] & [0] & [0] & [0] & [F_{23}^3] & [0] & [G_{23}^3] & [F_{33}^3] \end{bmatrix} \begin{Bmatrix} \{t_{11}^1\} \\ \{t_{12}^1\} \\ \{t_{13}^1\} \\ \{q_{21}^1\} \\ \{t_{22}^2\} \\ \{t_{23}^2\} \\ \{q_{31}^1\} \\ \{q_{32}^2\} \\ \{t_{33}^3\} \end{Bmatrix}$$

$$= \begin{bmatrix} [G_{11}^1] & [0] & [0] & [0] & [0] & [0] & [0] & [0] & [0] \\ [0] & [0] & [0] & [0] & [G_{22}^2] & [0] & [0] & [0] & [0] \\ [0] & [0] & [0] & [0] & [0] & [0] & [0] & [0] & [G_{33}^3] \end{bmatrix} \begin{Bmatrix} \{q_{11}^1\} \\ \{0\} \\ \{0\} \\ \{0\} \\ \{q_{22}^2\} \\ \{0\} \\ \{0\} \\ \{0\} \\ \{q_{33}^3\} \end{Bmatrix} \tag{12}$$

The matrix equation (12) is actually a hypermatrix with matrices for its entries. Likewise, the overall vectors shown have vectors for their entries. The blocked sparsity characteristic of the matrices that result from the multizone BEA approach is clearly evident from the zero blocks present in Eq. (12). When multizone techniques are employed, a number of significantly beneficial characteristics[37] are shown to be imparted to the BEA process.

Boundary Element Substructuring

Condensation of degrees of freedom in BEA[36-38] can be introduced by considering the matrix equations for a single zone. Reordering degrees of freedom and partitioning Eq. (10) into blocks that correspond to master degrees of freedom and degrees of freedom that could be condensed, one obtains

$$\begin{bmatrix} [F_{MM}] & [F_{MC}] \\ [F_{CM}] & [F_{CC}] \end{bmatrix} \begin{Bmatrix} \{t_M\} \\ \{t_C\} \end{Bmatrix} = \begin{bmatrix} [G_{MM}] & [G_{MC}] \\ [G_{CM}] & [G_{CC}] \end{bmatrix} \begin{Bmatrix} \{q_M\} \\ \{q_C\} \end{Bmatrix}$$

$$+ \begin{Bmatrix} \{f_M\} \\ \{f_C\} \end{Bmatrix} \tag{13a}$$

(13b)

The additional right-hand-side vector is included to account for additional thermal effects that might be present, such as

Given the zone matrix partitions $[F_{MM}]$, $[F_{CM}]$, $[F_{MC}]$, $[F_{CC}]$, $[G_{MM}]$, $[G_{CM}]$
and the vectors $\{v_1\} = [G_{CC}]\{q_C\}$, $\{v_2\} = [G_{MC}]\{q_C\}$, $\{f_M\}$, $\{f_C\}$

Form the triangular factorization of $[F_{CC}] = [L_{CC}][U_{CC}]$

Solve $[F_{CC}][D] = [F_{CM}]$ for $[D]$; and **Form** $[M_1] = [F_{MM}] - [F_{MC}][D]$

Solve $[F_{CC}][D] = [G_{CM}]$ for $[D]$; and **Form** $[M_2] = [G_{MM}] - [F_{MC}][D]$

Solve $[F_{CC}]\{d\} = \{v_1\}$ for $\{d\}$; and **Form** $\{v_C\} = \{v_2\} - [F_{MC}]\{d\}$

Solve $[F_{CC}]\{d\} = \{f_C\}$ for $\{d\}$; and **Form** $\{v_3\} = -[F_{CM}]\{d\}$

Form $\{v_C\} = \{v_C\} + \{v_3\} + \{f_M\}$

a) Boundary element zone condensation procedure.

Given the zone matrix partitions $[F_{CM}]$, $[G_{CM}]$
and the triangular factorization of $[F_{CC}] = [L_{CC}][U_{CC}]$
and the vectors $\{v_1\}$, $\{q_M\}$, $\{t_M\}$, $\{f_C\}$

Form $\{v\} = [G_{CM}]\{q_M\} + \{v_1\} - [F_{CM}]\{t_M\} + \{f_C\}$

Solve $[F_{CC}]\{t_C\} = \{v\}$ for $\{t_C\}$

b) Boundary element substructure expansion proceedure.

Fig. 3 Boundary-element substructure condensation and expansion algorithms.

internal heat generation. Solving the matrix equation (13b) for $\{t_C\}$ yields

$$\{t_C\} = [F_{CC}]^{-1}[G_{CM}]\{q_M\} + [F_{CC}]^{-1}[G_{CC}]\{q_C\} - [F_{CC}]^{-1}[F_{CM}]\{t_M\} + [F_{CC}]^{-1}\{f_C\} \quad (14)$$

Substituting Eq. (14) into the matrix equation (13a) and collecting terms yields

$$[M_1]\{t_M\} = [M_2]\{q_M\} + [M_3]\{q_C\} + [M_4]\{f_C\} + \{f_M\} \quad (15)$$

where

$$[M_1] = [F_{MM}] - [F_{MC}][F_{CC}]^{-1}[F_{CM}]$$
$$[M_2] = [G_{MM}] - [F_{MC}][F_{CC}]^{-1}[G_{CM}]$$
$$[M_3] = [G_{MC}] - [F_{MC}][F_{CC}]^{-1}[G_{CC}]$$
$$[M_4] = -[F_{MC}][F_{CC}]^{-1} \quad (16)$$

Equation (15) is called a condensed boundary-element zone matrix equation, whereas Eq. (14) is called a boundary-element zone matrix expansion equation.

Figure 2 illustrates the relative sizes of the matrices and vectors present in the BEA zone substructuring process. This figure, along with substructuring equations, helps to describe the BEA zone first-level assembly algorithm, and also the subsequent, optional condensation step. This first-level assembly algorithm requires that accounting be performed to indicate the appropriate partition destinations for all boundary-element contributions to the individual zone system matrices. These contributions can then be assembled with due regard for the boundary conditions present in the model, and by requiring that the individual zone's row sum[1-3] be used to determine the diagonal block entries in the $[F]$ matrix shown in Fig. 2.

Note that whenever the symbol $[F_{CC}]^{-1}$ appears in these equations, it always premultiplies either a column vector or rectangular matrix. The use of this matrix inversion notation is purely symbolic. In the computer implementation, no matrix inversion is ever performed. Instead, the triangular factorization of the matrix block $[F_{CC}]$ is performed once, and subsequently, these factors are used to solve the matrix equations shown next. This is possible because

$$\{d\} = [F_{CC}]^{-1}\{v\} \Rightarrow [F_{CC}]\{d\} = \{v\} \quad (17)$$

$$[D] = [F_{CC}]^{-1}[V] \Rightarrow [F_{CC}][D] = [V] \quad (18)$$

In Eq. (18) the rectangular matrix $[D]$ is a collection of column vectors $\{d_i\}$ that are formed from the forward reduction and backward substitution of the column vectors $\{v_i\}$ collected in the rectangular matrix $[V]$.

$$[D] = [\{d_1\},\{d_2\},\ldots,\{d_N\}]$$
$$[V] = [\{v_1\},\{v_2\},\ldots,\{v_N\}] \quad (19)$$

As shown in Ref. 37, it is possible to save significant computer storage space and data movement in the implementation by avoiding the storage of the rectangular matrices $[G_{MC}]$ and $[G_{CC}]$, as

$$[M_1]\{t_M\} = [M_2]\{q_M\} + \{v_C\} + [M_4]\{f_C\} + \{f_M\} \quad (20)$$

$$\{v_C\} = [G_{MC}]\{q_C\} - [F_{MC}][F_{CC}]^{-1}[G_{CC}]\{q_C\} \quad (21)$$

where

$$\{t_C\} = [F_{CC}]^{-1}[G_{CM}]\{q_M\} + [F_{CC}]^{-1}\{v_1\} - [F_{CC}]^{-1}[F_{CM}]\{t_M\} + [F_{CC}]^{-1}\{f_C\} \quad (22)$$

$$\{v_1\} = [G_{CC}]\{q_C\} \quad (23)$$

Figures 3a and 3b illustrate the steps involved in the computer implementation of the formulation.

A natural way to combine substructuring with multizone BEA capability is to allow for the possible condensation of degrees of freedom that appear exclusively in any particular boundary-element zone. In this case, the partitions to be eliminated by the condensation process coincide exactly with certain partitions already present in the multizone BEA procedure. This approach is also very natural from a modeling perspective, since entire boundary-element zones can be easily and arbitrarily identified for either condensation or no condensation, and also for subsequent expansion if they are to be condensed. When zones can be arbitrarily selected for condensation, a second-level assembly procedure for the formation of the overall sparse blocked system of equations must be able to assemble condensed or uncondensed zone contributions to the overall matrix system of equations.

The impact of the BEA zone condensation technique, when employed in nonlinear heat transfer, can be explained by considering the two-zone example problem shown in Fig. 4. Here the nonlinear boundary condition is confined exclusively to zone two. This two-zone model produces the sparse blocked left-hand-side matrix also shown in Fig. 4. In this figure, the changing entries in the left-hand-side matrix due to the temperature-dependent convection coefficient are highlighted using diagonal crosshatching. A second matrix is shown in Fig. 4 that corresponds to the overall left-hand-side matrix for the case where zone one has been condensed. Comparison of these two matrices shows very clearly why the iterative process associated with the evolution of this class of nonlinear problem can be performed in a more economical fashion when condensation is employed. Even when methods are used that do not alter the left-hand-side matrices in each iteration, these methods are faster due to the fact that a smaller LU decomposition is employed in each stage of the iterative process. The advantage of the multizone BEA and zone condensation techniques will also be shown to extend to the DSA process described in this paper.

Nonlinear Design Sensitivity Analysis Formulation

Solution of the resulting nonlinear set of algebraic equations can be accomplished by an iterative technique consisting of an initial guess at surface temperature at nodes with temperature-dependent convection or radiation boundary conditions, computation of the equivalent $h(T)$, and assembly of the matrix equations corresponding to Eq. (7). The left-hand-side matrix is then factored, and forward reduction and back substitution are accomplished with the right-hand-side vector to obtain an updated response vector. This response is then used to repeat the entire process until convergence. The overall process can be characterized by an expression similar to Eq. (3).

$$[A]^{(M-1)}\{x\}^{(M)} = \{b\}^{\{M-1\}} \tag{24}$$

The superscript notation is used to convey the fact that temperatures obtained in the $M-1$th iteration are used to construct the left-hand-side matrix $[A]$ and the right-hand-side vector $\{b\}$ to predict the response in iteration M.

An effective DSA formulation for this nonlinear problem can be developed by performing implicit differentiation of the *converged* Eq. (24) with respect to the Lth design variable X_L. That is to say, during the analysis phase of the nonlinear thermal problem, the matrix $[A]^{(M-1)}$ is evolved to its "correct" state, with all temperatures used to make the h coefficients at their converged values. The resulting sensitivity equations are

$$\frac{\partial}{\partial X_L}([A]\{x\} = \{b\}) \Rightarrow [A]_{,L}\{x\} + [A]\{x\}_{,L} = \{b\}_{,L}$$

or

$$[A]\{x\}_{,L} = (\{b\}_{,L} - [A]_{,L}\{x\}) \tag{25}$$

A representative three-degree-of-freedom example system is shown next, with node 2 the node with a radiation boundary condition. The case of a temperature-dependent convection boundary condition would be the same, except the symbol $h(T)$ would replace the symbol $h_r(T)$ shown in these equations.

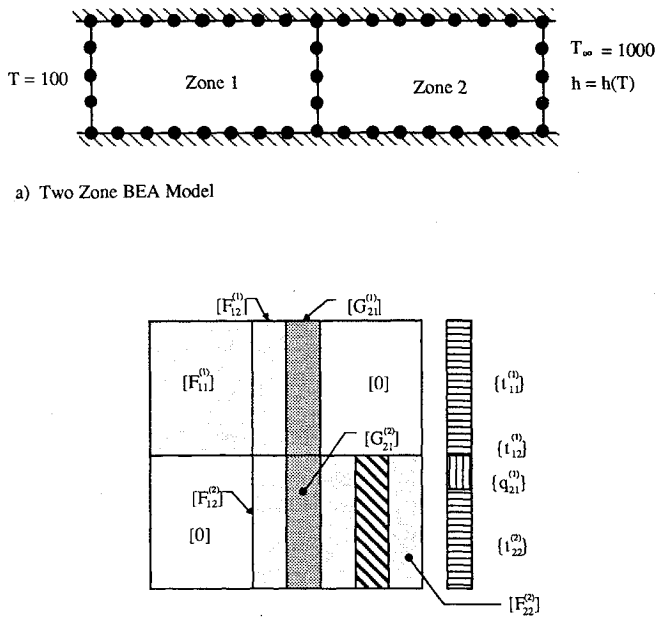

Fig. 4 Matrices involved in example two-zone problem.

$$\begin{Bmatrix} f_{11} & [f_{12} - g_{12}h_r(T)] & f_{13} \\ f_{21} & [f_{22} - g_{22}h_r(T)] & f_{23} \\ f_{31} & [f_{32} - g_{32}h_r(T)] & f_{33} \end{Bmatrix} \begin{Bmatrix} T_{1,L} \\ T_{2,L} \\ T_{3,L} \end{Bmatrix} = \begin{bmatrix} g_{11,L} & g_{12,L} & g_{13,L} \\ g_{21,L} & g_{22,L} & g_{23,L} \\ g_{31,L} & g_{32,L} & g_{33,L} \end{bmatrix} \begin{Bmatrix} q_1 \\ -h_r(T)T_\infty \\ q_3 \end{Bmatrix}$$

$$+ \begin{bmatrix} g_{11,L} & g_{12,L} & g_{13,L} \\ g_{21,L} & g_{22,L} & g_{23,L} \\ g_{31,L} & g_{32,L} & g_{33,L} \end{bmatrix} \begin{Bmatrix} 0 \\ -h_{r,L}(T)\ T_\infty \\ 0 \end{Bmatrix} - \begin{Bmatrix} f_{11,L} & [f_{12,L} - g_{12,L}h_r(T) - g_{12}h_{r,L}(T)] & f_{13,L} \\ f_{21,L} & [f_{22,L} - g_{22,L}h_r(T) - g_{22}h_{r,L}(T)] & f_{23,L} \\ f_{31,L} & [f_{32,L} - g_{32,L}h_r(T) - g_{32}h_{r,L}(T)] & f_{33,L} \end{Bmatrix} \begin{Bmatrix} T_1 \\ T_2 \\ T_3 \end{Bmatrix} \tag{26}$$

Note that the left-hand-side matrix shown in this equation is indeed the *converged* $[A]^{(M-1)}$ matrix, formed and factored during the previous nonlinear thermal analysis step. The first two terms shown on the right of Eq. (26) are $\{b\}_{,L}$. The last term on the right is $[A]_{,L}\{x\}$, which involves $f_{ij,L}$ and $g_{ij,L}$. As shown in Refs. 32–36, these sensitivity coefficients can be obtained using analytical derivatives of the BEA kernel functions with respect to shape design variables.

For radiation boundary conditions, one can differentiate the relation for h_r shown in Eq. (9) to obtain and expression for the sensitivity of the convection coefficient to X_L.

$$h_{r,L}(T) = \sigma E T_{,L}(3T^2 + 2TT_r + T_r^2) \tag{27}$$

In this expression, it is assumed that the radiation view factor is insensitive to changes in the design variable. A formula involving $E_{,L}$ could also be employed in a straightforward manner. For temperature-dependent convection boundary conditions, the exact form of the DSA equations will depend on the equation used to model the convection coefficient's variation with temperature. The general form of the relation is expressed as

$$[q = h(T - T_\infty)]_{,L}$$

$$q_{,L} = h_{,L}(T - T) + h(T_{,L} - T_\infty) \tag{28}$$

A group of relationships can be considered by using the cubic equation shown in Eqs. (29) and (30). Notice that this relation includes the cubic radiation boundary condition as a special case.

$$[h(T) = aT^3 + bT^2 + cT + d]_{,L} \tag{29}$$

$$h_{,L} = (3aT^2 + 2bT + c)T_{,L} \tag{30}$$

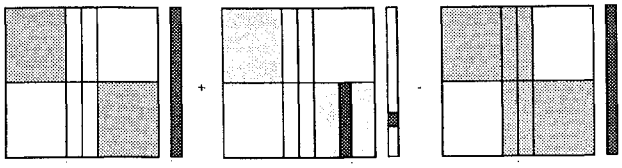

Three Terms That Comprise Right Hand Side Vector for DSA

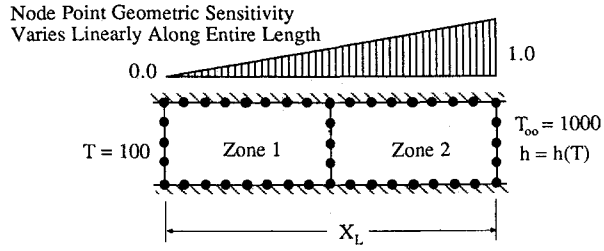

a) Two Zone BEA Model With Full Geometric Sensitivity

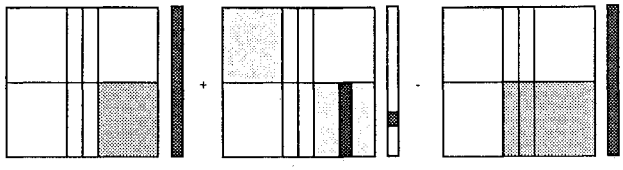

Three Terms That Comprise Right Hand Side Vector for DSA

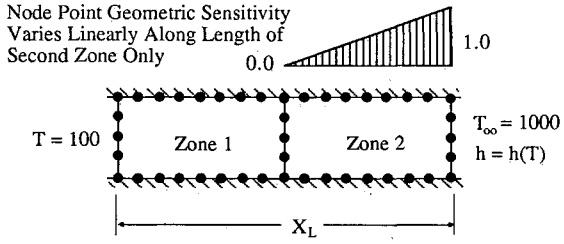

b) Two Zone BEA Model With Partial Geometric Sensitivity

Fig. 5 Matrices involved in two-zone sensitivity problem showing additional sparsity for partial geometric sensitivity.

This result allows for the generalization of Eq. (26) to include the general case of temperature-dependent convection by substituting $h(T)$ for all occurrences of $h_r(T)$ in this equation.

A fundamental observation regarding the solution of Eq. (26) is that $T_{,L}$ *appears on both sides of the equation.* Thus, it is a nonlinear equation that must be solved iteratively. However, Eq. (26) is far different from the nonlinear equation set solved in the previous thermal analysis. The left-hand-side matrix present in Eq. (26) is *correct*, having been constructed using the converged values of the thermal response. Also, this left-hand-side matrix has already been factored and can be saved from the last iteration of the previous thermal analysis and reused in the iterative process to evolve $T_{,L}$ to its converged state. *These iterations therefore involve only forward reduction and back substitution operations.* Symbolically, the solution of Eq. (26) can be characterized as

$$[A]\{x\}_L^{(M)} = \{c\}_L^{(M-1)} \tag{31}$$

To consider the contrasting situations that exist in nonlinear thermal analysis vs the nonlinear thermal DSA, Eq. (31) can be compared with Eq. (24). It is easily seen that the iterations characterized by Eq. (31) for the solution of the DSA problem should be far less computationally burdensome, because the left-hand-side matrix remains constant. In the numerical examples presented in this paper, this fact is demonstrated repeatedly.

Table 1 Timing statistics for rectangular bar example problem

Operation	CPU timings for major operations during analysis and design sensitivity analysis: Example 1.1[a]	Example 1.2[b]	Example 1.3[c]
	Analysis		
Preliminaries	0.9	2.0	2.0
Numerical integration	88.0	80.0	82.1
Assembly			
Oversight	0.1	0.0	0.2
Zone level	7.3	2.4	2.8
Overall system level	0.7	2.9	3.2
Triangular factorization	54.4	7.3	8.1
Forward reduction/ back substitution	6.8	5.9	6.3
Response recovery	2.7	3.7	4.3
	Design sensitivity analysis		
Preliminaries	0.1	0.0	0.0
Numerical integration	113.6	101.0	13.0
Assembly			
Oversight	1.7	4.3	3.5
Zone level	13.1	1.9	1.0
Overall system level	1.0	4.8	4.0
Forward reduction/ back substitution	8.5	7.1	5.8
Response recovery	2.9	4.0	4.0
Total	302.1	227.8	136.6

[a]Single-zone model.
[b]Five-zone model, full geometric sensitivity.
[c]Five-zone model, partial geometric sensitivity.

An additional benefit of multizone BEA that occurs in design sensitivity analysis can be explained with the aid of Fig. 5. In this figure, two boundary-element models are shown. Both models have their length controlled by the same design variable. The model shown in Fig. 5a is controlled by design variable X_L in such a fashion that the *geometric* sensitivity of the nodes varies in a linear manner over the entire length of the model. The three terms that contribute to the DSA right-hand-side vector associated with this model are also shown. This right-hand-side vector is the multizone equivalent of the right-hand side of Eq. (26). The matrices present in this DSA procedure have the same basic sparse blocked structure as their counterparts in the nonlinear thermal analysis. This situation can be contrasted by the model and its associated matrices shown in Figure 5b. This model is again controlled by a design variable X_L, but this time only the nodes in zone two are geometrically sensitive. Note that the matrices associated with this DSA problem have significant additional block sparsity. For this kind of problem, this sparsity can be exploited in the numerical integration and matrix-vector multiplication steps.

Numerical Results

A series of test cases were executed to demonstrate the efficiency and accuracy of the DSA formulations and characterize their implementations. All computations were conducted on the same computer with the same Fortran 77 compiler. Classical closed-form solutions to nonlinear thermal problems were differentiated to derive exact expressions for the rates of change of the thermal response to changes in design variables. An example problem without a closed-form solution is also included to demonstrate the characteristics of the DSA procedure on a larger-scale problem. In this case, the answers computed by the DSA program were compared to sensitivities obtained by a finite-difference procedure.

Rectangular Bar Subjected to Temperature-Dependent Convection Boundary Conditions

The rectangular bar shown in Fig. 6 was analyzed using three different boundary-element models. The single-zone

model (example problem 1.1) shown in this figure contains 80 nodes and 40 three-node quadratic boundary elements. The five-zone model (example problems 1.2 and 1.3) shown in Figs. 6b and 6c has 92 nodes and 56 quadratic boundary elements. This bar has a unit conductivity and is insulated along its top and bottom surfaces, maintained at a uniform temperature of 100°C at its left end, and subjected to a nonlinear convection boundary condition along its right end surface. The bulk temperature associated with the convection boundary condition is 400°C and h was chosen to be a linear function of the unknown surface temperature as shown here.

$$h(T) = 2.5 - \frac{2}{400}(T - 400) \tag{32}$$

The design variable X_L in this example problem controls the length of the bar. Although X_L is the same in all three example problems presented in this section, the geometry of the nodes is controlled differently in example problem 1.3 than in the other two example problems, as shown in Fig. 6. The horizontal location of the nodes varies linearly over the entire length of the rod for example problems 1.1 and 1.2. In example problem 1.3, the horizontal geometric sensitivity of the nodes in the model is zero in the first four zones and varies linearly in the last zone. This third example problem points out the fact that the same geometric detail (in this case, the length of the rod) can be controlled by a design variable in ways that can limit geometric sensitivity to impart additional matrix sparsity during DSA, as discussed in previous sections of this paper.

The three different nonlinear analyses and design sensitivity analyses previously described were performed for this physical problem. These different cases are characterized in the first part of Table 1, with the latter part of this table containing CPU timing information for the major steps in the iterative process required to evolve the problems to their converged solutions. Insights about the performance of multizone thermal BEA and DSA technique in the nonlinear thermal analysis context can be gained by consideration of these tabulated results. Table 2 contains a comparison of exact and computed sensitivities for these problems. A number of comments can be made regarding these examples: 1) The accuracy of the computed sensitivities is remarkably good. 2) Multizone models use considerably less storage (3480 words) than their single-zone counterparts (6400 words) in this example. 3) The multizone approach seems to have absolutely no effect on the *rate* of convergence of the nonlinear iterative process, both for the analysis and the DSA. The single-zone analysis took four iterations, whereas the multizone analyses took three iterations each. Both the single- and multizone sensitivity analyses converged in five iterations. This effect is verified by all of the example problems presented. 4) The CPU time required in the factorization of the left-hand-side matrix performed in the analysis step is drastically reduced when the multizone models are employed. 5) The matrix sparsity imparted to the sensitivity matrices in example 1.3 causes significant reduction in the

Table 2 Accurary comparison for rectangular bar shape sensitivity example problem with temperature dependent convection boundary conditions

			Five-zone model with full geometric sensitivity			
			$T_{,L} \times 10^{-3}$		$q_{,L} \times 10^{-2}$	
Point	x	$x_{,L}$	Exact	Computed	Exact	Computed
1	0.0	0.0	0.0	0.0	0.23096	0.23095
2	80.0	0.22222	0.20482	0.20432	0.23096	0.23097
3	160.0	0.44444	0.40965	0.40863	0.23096	0.23097
4	240.0	0.6667	0.61448	0.61295	0.23096	0.23097
5	320.0	0.88889	0.81931	0.81720	0.23096	0.23097
6	330.0	0.91667	0.84491	0.84472	0.23096	——[a]
7	340.0	0.94444	0.87052	0.86989	0.23096	——
8	350.0	0.97222	0.89612	0.89514	0.23096	——
9	360.0	1.0	0.92172	0.92270	0.23096	0.23097
			Five-zone model with partial geometric sensitivity			
			$-T_{,L}$		$q_{,L} \times 10^{-2}$	
Point	x	$x_{,L}$	Exact	Computed	Exact	Computed
1	0.0	0.0	0.0	0.0	0.23096	0.23098
2	80.0	0.0	0.18477	0.18478	0.23096	0.23096
3	160.0	0.0	0.36954	0.36957	0.23096	0.23096
4	240.0	0.0	0.55432	0.55435	0.23096	0.23096
5	320.0	0.0	0.73909	0.73913	0.23096	0.23101
6	330.0	0.25	0.55409	0.55412	0.23096	——
7	340.0	0.50	0.36908	0.36910	0.23096	——
8	350.0	0.75	0.18408	0.18409	0.23096	——
9	360.0	1.0	−0.00092172	−0.00092328	0.23096	0.23113

[a]No heat flux computed at this location.

Table 3 Accuracy comparison for rectangular bar shape sensitivity example problem with radiation boundary conditions

			Five-zone model with full geometric sensitivity			
			$T_{,L} \times 10^{-3}$		$q_{,L} \times 10^{-2}$	
Point	x	$x_{,L}$	Exact	Computed	Exact	Computed
1	0.0	0.0	0.0	0.0	0.23118	0.23095
2	80.0	0.22222	0.11832	0.11678	0.23118	0.23119
3	160.0	0.44444	0.23665	0.23356	0.23118	0.23119
4	240.0	0.66667	0.35498	0.35035	0.23118	0.23119
5	320.0	0.88889	0.47330	0.46711	0.23118	0.23119
6	330.0	0.91667	0.48809	0.48393	0.23118	——[a]
7	340.0	0.94444	0.50288	0.49854	0.23118	——
8	350.0	0.97222	0.51767	0.51341	0.23118	——
9	360.0	1.0	0.53247	0.53037	0.23118	0.23121
			Five-zone model with partial geometric sensitivity			
			$-T_{,L}$		$q_{,L} \times 10^{-2}$	
Point	x	$x_{,L}$	Exact	Computed	Exact	Computed
1	0.0	0.0	0.0	0.0	0.23118	0.23120
2	80.0	0.0	0.18494	0.18496	0.23118	0.23118
3	160.0	0.0	0.36989	0.36992	0.23118	0.23118
4	240.0	0.0	0.55484	0.55488	0.23118	0.23118
5	320.0	0.0	0.73979	0.73984	0.23118	0.23122
6	330.0	0.25	0.55471	0.55475	0.23118	——
7	340.0	0.50	0.36963	0.36956	0.23118	——
8	350.0	0.75	0.18454	0.18456	0.23118	——
9	360.0	1.0	−0.00053247	−0.00053229	0.23118	0.23146

[a]No heat flux computed at this location.

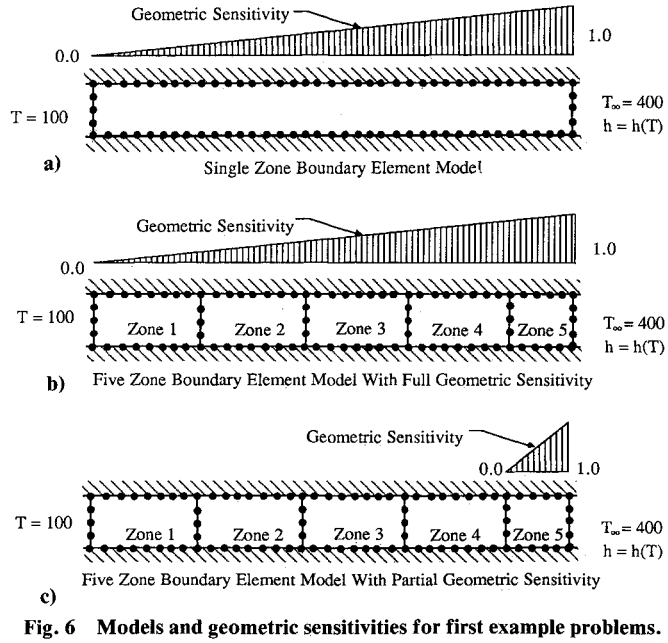

Fig. 6 Models and geometric sensitivities for first example problems.

Table 4 Timing statistics for circular plate with central hole example problem

Operation	CPU timings for major operations during analysis and design sensitivity analysis			
	Example 2.1[a]	Example 2.2[b]	Example 2.3[c]	Example 2.3[d]
	Analysis			
Preliminaries	0.6	0.7	0.9	0.8
Numerical integration	33.4	36.5	35.9	35.5
Assembly				
Oversight	0.0	0.1	0.0	0.2
Zone level	2.7	2.2	1.5	1.6
Overall system level	0.6	2.0	1.9	2.2
Triangular factorization	10.2	7.4	3.4	4.1
Forward reduction/ back substitution	4.4	5.4	5.1	5.8
Response recovery	1.4	1.7	1.7	2.1
	Design Sensitivity Analysis			
Preliminaries	0.0	0.0	0.0	0.0
Numerical integration	45.2	47.2	47.5	14.9
Assembly				
Oversight	0.9	1.1	2.5	2.1
Zone level	6.5	5.8	2.1	2.2
Overall system level	0.8	3.4	3.2	2.7
Forward reduction/ back substitution	4.5	5.4	5.0	4.6
Response recovery	0.6	0.7	0.7	0.7
Total	111.4	119.5	111.2	79.2

[a]Single-zone model.
[b]Two-zone model, full geometric sensitivity.
[c]Three-zone model, full geometric sensitivity.
[d]Three-zone model, partial geometric sensitivity.

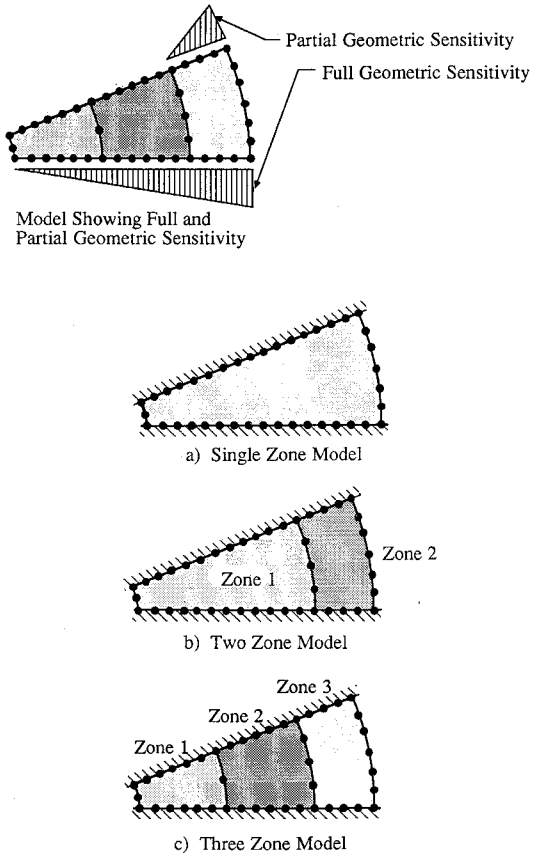

Fig. 7 Boundary-element models for second example problems.

time required to numerically integrate their contributions (13.0 s instead of either 101.0 or 113.6 s).

Rectangular Bar Subjected to Radiation Boundary Conditions

The five-zone models shown in Figs. 6b and 6c were used to study the accuracy and efficiency of the DSA formulation for a problem with radiation boundary conditions. These example problems are referred to as example problems 1.4 and 1.5, respectively. In this case, the left end of the rod was maintained at a uniform temperature of 100 K while the right end was subjected to a radiation boundary condition quantified by $\sigma = 5.67 \times 10^{-8}$, $E = 0.3$, and $T_r = 400.0$ The CPU timing and storage statistics for these runs were very similar to those reported in example problems 1.2 and 1.3. Table 3 contains a comparison of exact and computed sensitivities for these problems. The accuracies of the computed nonlinear thermal response sensitivities are again seen to be excellent.

Circular Plate with Central Hole Subjected to Temperature-Dependent Convection Boundary Conditions

As a second example, the three boundary-element models shown in Fig. 7 were used in a nonlinear thermal analysis and sensitivity analysis. These partial models are used to represent a generic segment of a circular plate with a central hole. The single-zone model (example problem 2.1) has 40 nodes and 20 three-node quadratic boundary elements, the two-zone model (example problem 2.3) has 44 nodes and 26 quadratic elements. The model was first subjected to a convection boundary condition at its outer radius that has a coefficient that was a quadratic function of the surface temperature as described by

$$h(T) = \frac{3}{450^2}(T + 50)^2 + 1 \tag{33}$$

The bulk temperature associated with this boundary condition was 70 K and the conductivity was set equal to unity. The

Table 5 Accuracy comparison for circular plate with central hole shape sensitivity example problem with temperature-dependent convection boundary conditions

Three-zone model with full geometric sensitivity

			$-T,_L$		$q,_L$	
Point	R	$R,_L$	Exact	Computed	Exact	Computed
1	4.0	0.0	0.0	0.0	4.1327	4.0516
2	5.0	0.0625	3.3653	3.3785	4.7170	——[a]
3	6.0	0.125	5.0541	5.0731	4.7146	——
4	7.0	0.1875	5.8649	5.8855	4.5210	——
5	8.0	0.25	6.1768	6.1974	4.2708	——
6	9.0	0.3125	6.1892	6.2091	4.0139	——
7	10.0	0.375	6.0151	6.0348	3.7693	3.7718
8	11.0	0.4375	5.7221	5.7390	3.5432	——
9	12.0	0.5	5.3525	5.3671	3.3370	——
10	13.0	0.5625	4.9337	4.9462	3.1499	——
11	14.0	0.625	4.4838	4.4943	2.9803	——
12	15.0	0.6875	4.0151	4.0237	2.8264	——
13	16.0	0.75	3.5360	3.5432	2.6865	2.6880
14	17.0	0.8125	3.0525	3.0580	2.5589	——
15	18.0	0.875	2.5687	2.5726	2.4424	——
16	19.0	0.9375	2.0874	2.0898	2.3355	——
17	20.0	1.0	1.6108	1.6188	2.2373	2.2385

Three-zone model with partial geometric sensitivity

			$T,_L$		$q,_L$	
Point	R	$R,_L$	Exact	Computed	Exact	Computed
1	4.0	0.0	0.0	0.0	4.1327	4.0516
2	5.0	0.0	3.6888	3.6901	3.3062	——
3	6.0	0.0	6.7027	6.7049	2.7551	——
4	7.0	0.0	9.2510	9.2529	2.3615	——
5	8.0	0.0	11.458	11.460	2.0663	——
6	9.0	0.0	13.405	13.407	1.8367	——
7	10.0	0.0	15.147	15.148	1.6531	1.6527
8	11.0	0.0	16.722	16.723	1.5028	——
9	12.0	0.0	18.161	18.161	1.3775	——
10	13.0	0.0	19.484	19.484	1.2716	——
11	14.0	0.0	20.709	20.709	1.1807	——
12	15.0	0.0	21.850	21.849	1.1020	——
13	16.0	0.0	22.916	21.915	1.0331	1.0323
14	17.0	0.25	15.620	15.619	1.4605	——
15	18.0	0.50	9.1881	9.1874	1.7892	——
16	19.0	0.75	3.4815	3.4814	2.0424	——
17	20.0	1.0	− 1.6108	− 1.6105	2.2373	2.2369

[a]No heat flux computed at this location.

straight sides of these models were given an adiabatic boundary condition to simulate the axisymmetric characteristics of the response. The surface located at the inner radius was maintained at a temperature of 1000 K.

The design variable chosen in this set of example problems is the outer radius of the circular plate. The first three example problems described in this section are controlled by this design variable in such a manner that the nodes in the model have radial geometric sensitivity that varies linearly from zero at the inner radius to 1 on the outer radius. A fourth problem (example problem 2.4) is included that consists of the three-zone model with node point geometric sensitivity varying linearly from zero at the zone 2-3 interface to 1 at the outer radius. Thus, this example problem includes geometrically insensitive boundary-element zones. The geometric sensitivities of these four models are also displayed in Fig. 7.

The four different analyses and design sensitivity analyses just discussed were performed for this physical problem. The resulting CPU timings are shown in the bottom part of Table 4. Table 5 contains a comparison of exact and computed sensitivities for these problems. A number of comments can be made about the performance of the nonlinear procedures in this example. 1) The accuracy of the computed sensitivities is excellent. 2) The multizone techniques again had no impact on the rate of convergence of the iterative solution strategy for either the analysis or DSA. The single-zone and multizone analyses each took six iterations to converge. Both the single- and multizone sensitivity analyses converged in nine iterations. 3) Multizone models again used less storage (1464 words for the two-zone model and 1186 words for the three zone model) than their single-zone counterparts (1600 words) in this example. 4) The CPU time required in the factorization of the left-hand-side matrix performed in the analysis step is reduced by more than a factor of 2 when the multizone models are employed. However, this problem is so small that the factorization time is a relatively small fraction of the time consumed by the overall procedure. 5) The matrix sparsity imparted to the sensitivity matrices in example 2.4 causes a significant reduction in the time required to numerically integrate their contributions (14.9 s instead of 45.2, 47.2, and 47.5 s for the fully sensitive models).

Circular Plate with Central Hole Subjected to Radiation Boundary Conditions

The three-zone boundary-element model shown in Fig. 7c was used again in two nonlinear thermal analyses and design sensitivity analyses with a radiation boundary condition on the surface located at the outer radius of the circular plate. The design variable and geometric sensitivities used were the same as those employed in example problems 2.3 and 2.4. These problems are referred to as example problems 2.5 and 2.6, respectively. The temperature of the radiating body was specified to be 2000 K and $\sigma = 5.67 \times 10^{-8}$ and $E = 0.3$. The inner radius of the cylinder was maintained at 1000 K in this example. The CPU timing and storage statistics associated with these analysis runs were similar to those reported in Table 4 for problems 2.3 and 2.4. Table 6 contains a comparison of exact and computed sensitivities for these two problems. As in the previous examples, the computed sensitivities are in excellent agreement with the exact solutions.

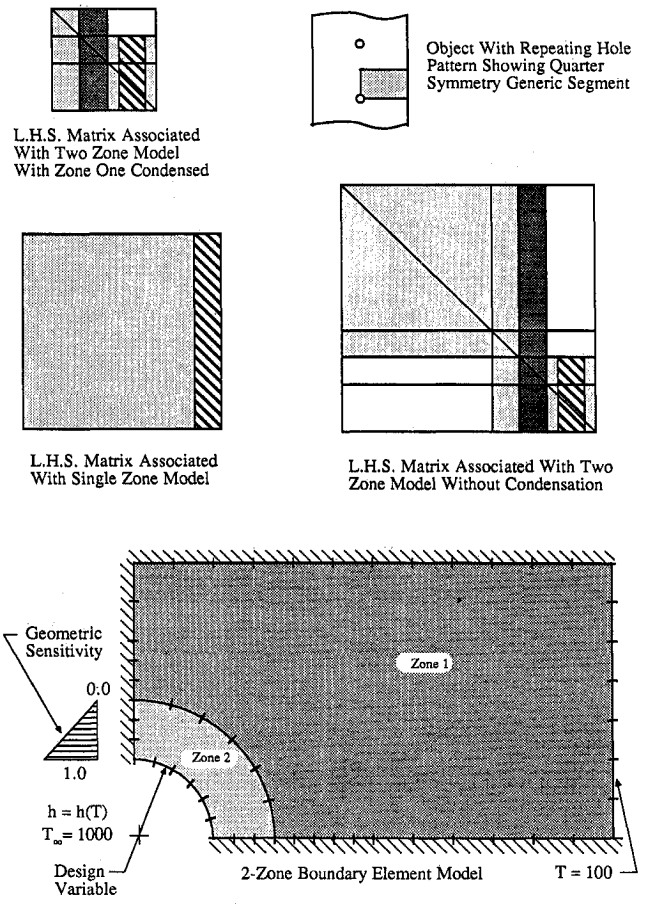

Fig. 8 Boundary-element model and left-hand-side matrices for third example problems.

Table 6 Accuracy comparison for circular plate with central hole shape sensitivity example problem with radiation boundary conditions

			$-T_{,L}$		$-q_{,L}$	
Point	R	$R_{,L}$	Exact	Computed	Exact	Computed
	Three-zone model with full geometric sensitivity					
1	4.0	0.0	0.0	0.0	4.8251	4.7450
2	5.0	0.0625	3.4594	3.4741	5.4133	——[a]
3	6.0	0.125	5.1179	5.1394	5.3740	——
4	7.0	0.1875	5.8410	5.8643	5.1346	——
5	8.0	0.25	6.0374	6.0608	4.8395	——
6	9.0	0.3125	5.9214	5.9442	4.5415	——
7	10.0	0.375	5.6137	5.6366	4.2599	4.2624
8	11.0	0.4375	5.1862	5.2062	4.0010	——
9	12.0	0.5	4.6835	4.7011	3.7656	——
10	13.0	0.5625	4.1343	4.1497	3.5526	——
11	14.0	0.625	3.5574	3.5708	3.3598	——
12	15.0	0.6875	2.9654	2.9769	3.1851	——
13	16.0	0.75	2.3670	2.3771	3.0265	3.0278
14	17.0	0.8125	1.7679	1.7762	2.8820	——
15	18.0	0.875	1.1723	1.1787	2.7501	——
16	19.0	0.9375	0.5830	0.5875	2.6293	——
17	20.0	1.0	0.00177	0.00463	2.5182	2.5211
	Three-zone model with partial geometric sensitivity					
1	4.0	0.0	0.0	0.0	4.8251	4.8380
2	5.0	0.0	4.3068	4.3081	3.8601	——[a]
3	6.0	0.0	7.8257	7.8274	3.2167	——
4	7.0	0.0	10.800	10.803	2.7572	——
5	8.0	0.0	13.378	13.380	2.4125	——
6	9.0	0.0	15.651	15.652	2.1445	——
7	10.0	0.0	17.685	17.685	1.9300	1.9294
8	11.0	0.0	19.524	19.524	1.7546	——
9	12.0	0.0	21.203	21.202	1.6083	——
10	13.0	0.0	22.748	22.747	1.4846	——
11	14.0	0.0	24.179	24.177	1.3786	——
12	15.0	0.0	25.510	25.508	1.2867	——
13	16.0	0.0	26.756	26.752	1.2062	1.2046
14	17.0	0.25	18.789	18.786	1.6727	——
15	18.0	0.50	11.771	11.768	2.0310	——
16	19.0	0.75	5.5482	5.5450	2.3066	——
17	20.0	1.0	−0.00177	−0.00463	2.5182	2.5182

[a]No heat flux computed at this location.

Larger Problem with Nonlinear Convection Boundary Condition

Figure 8 depicts a quarter-symmetry BEA model of the generic repeated segment of a long rectangular strip containing a regular pattern of holes. This component is subjected to a temperature-dependent convection boundary condition shown here on the curved surface of the hole with a bulk temperature of 1000 K.

$$H(T) = \frac{1}{800^2}(T + 100)^2 + 3 \tag{34}$$

The two vertical sides of this object are constrained to be at a constant temperature of 100 K. Symmetry is enforced in this model using the adiabatic boundary conditions. The conductivity in this component was taken to be unity, and the design variable is the radius of the hole. The geometric sensitivity of the nodes in the boundary-element model is also depicted in Fig. 8. Two different boundary-element models were used in this example problem. First, a single-zone model was used and the set of single-zone analysis and sensitivity analysis runs were performed. This problem is designated example problem 3.1. This set was then followed by another (example problems 3.2 and 3.3) in which the two-zone model shown in Fig. 8 was used. The two-zone model was run both with (example problem 3.3) and without (example problem 3.2) condensation of zone 1. CPU timing results of these analysis and sensitivity runs are listed in Table 7.

This example problem has no exact, closed-form solution. A finite-difference procedure was used to determine an approximate thermal response sensitivity for this problem's response sensitivities. The 0.1 step size was determined to be adequate for this approximation process. A comparison of the thermal response sensitivities computed using the formulation presented in this paper and those obtained via the finite-difference approximation is given in Table 8.

Table 7 Timing statistics for rectangular plate with central hole example problem

	CPU timings for major operations during analysis and design sensitivity analysis		
Operation	Example 3.1[a]	Example 3.2[b]	Example 3.3[c]
	Analysis		
Preliminaries	1.2	1.5	1.5
Numerical integration	98.3	113.9	113.2
Assembly			
Oversight	0.2	0.1	2.9
Zone level	9.9	8.9	3.6
Condensation (optional)	——	——	19.2
Overall system level	1.7	0.5	0.1
Triangular factorization	70.6	81.5	8.0
Forward reduction/ back substitution	8.3	5.9	3.1
Response recovery	3.0	1.4	1.4
	Design Sensitivity Analysis		
Preliminaries	0.0	0.0	0.0
Numerical integration	60.8	31.3	30.5
Assembly			
Oversight	5.0	5.8	5.8
Zone level	6.5	6.0	6.0
Overall system level	0.8	0.1	0.4
Forward reduction/ back substitution	24.2	13.2	8.3
Response recovery	1.3	0.7	0.7
Total	291.8	270.8	204.7

[a]Single-zone model.
[b]Two-zone model, no condensation.
[c]Three-zone model, condensation of zone 1.

Table 8 Accuracy comparison for rectangular plate with central hole shape sensitivity example problem with temperature-dependent convection boundary conditions

	$T_{,L}$		$q_{,L}$	
Point	Finite difference	Computed	Finite difference	Computed
1	1.8250	1.8955	——[a]	——
2	31.542	31.865	——	——
3	51.073	51.311	——	——
4	65.337	65.415	——	——
5	64.480	64.883	——	——
6	52.554	53.047	——	——
7	33.606	34.049	——	——
8	3.2884	3.3419	——	——
9	3.1789	3.2302	15.220	15.477
10	2.9208	2.9442	13.823	14.092
11	2.5137	2.5728	12.010	12.296
12	2.1572	2.2218	10.317	10.604
13	1.8988	1.9769	9.1349	9.4259
14	65.206	65.360	5.5706	5.6939
15	65.007	65.220	5.0880	5.0866
16	64.794	65.062	4.2197	4.2286
17	64.596	64.948	3.3014	3.3341
18	64.511	64.896	2.6034	2.6531

[a]Heat flux not computed at this point.

An itemized discussion of the performance of the nonlinear procedures in this example problem follows. 1) The multizone and condensation techniques again had no impact on the rate of convergence of the iterative solution strategy for either the analysis or DSA. In all example problems, the analysis converged in four iterations, whereas the sensitivity analysis converged in seven iterations. 2) Multizone models, this time, did not use less storage (8836 words for the one-zone model and 9554 words for the two-zone model) than their single-zone counterparts. 3) As in the first and second examples, conden-

sation is shown to significantly reduce the computer memory (2102 words) required to store the overall BEA left-hand-side matrix. 4) Zone condensation was again shown to reduce the CPU resources required to accomplish the iterative solution process. 5) Expansion of the response at the end of the iterative process to recover the temperatures and normal heat-flux components at the condensed degrees of freedom was accomplished in a very marginal amount of CPU time. 6) The accuracy of the computed sensitivities is again seen to be excellent.

Conclusions

A boundary-element formulation for the computation of thermal response shape sensitivities for objects subjected to nonlinear boundary conditions has been presented. The accuracy and efficiency of this approach have been demonstrated by the presentation of a number of example problems. The computationally effective techniques of multizone analysis and zone condensation have been shown to remain applicable in this nonlinear sensitivity analysis. It has thus been demonstrated that the implicit differentiation approach to design sensitivity analysis using a boundary-element formulation is extendable to effectively treat nonlinear problems.

Acknowledgments

Portions of the research discussed herein have been supported by a grant from the U.S. National Science Foundation (DDM-8996171) and the NASA Lewis Research Center (NAG 3-1089) to Clarkson University. Any opinions, findings, and conclusions or recommendations expressed in this publication are those of the authors and do not reflect the views of these other organizations.

References

[1]Banerjee, P. K., and Butterfield, R., *Boundary Element Methods in Engineering Science*, McGraw-Hill, London, 1981.

[2]Brebbia, C. C., and Walker, S., *Boundary Element Techniques in Engineering*, Newnes Butterworths, London, 1980.

[3]Brebbia, C. A., Telles, J. C. F., and Wrobel, L. C., *Boundary Element Techniques*, Springer-Verlag, Berlin, 1984.

[4]Skerget, P. and Brebbia, C. A., "Nonlinear Potential Problems," *Progress in Boundary Element Methods*, Vol. 2, Springer-Verlag, New York, 1983.

[5]Anza, J. J., Ahedo, E., Da Riva, I., and Alarcon, E., "A New Boundary Condition Solved With BEM," *Boundary Element Methods in Engineering*, edited by C. Brebbia, Springer-Verlag, Berlin, 1982, pp. 607-618.

[6]Bialecki, R., and Nowak, A. J., "Boundary Value Problems for Nonlinear Boundary Conditions," *Applied Mathematical Modelling*, Vol. 5, No. 6, 1981, pp. 417-421.

[7]Akkuratov, Y. N., and Mikhailov, V. N., "The Method of Boundary Integral Equations for the Solution of Nonlinear Heat Transmission Problems," *USSR Computational Mathematics and Mathematical Physics*, Vol. 20, 1980, pp. 117-125.

[8]Onishi, K., and Kuroki, T., "Boundary Element Method in Singular and Nonlinear Heat Transfer," *Boundary Element Methods in Engineering*, edited by C. Brebbia, Springer-Verlag, Berlin, 1982, pp. 141-155.

[9]Butterfield, R., "An Application of the Boundary Element Method to Potential Flow Problems in Generally Inhomogeneous Bodies," *Recent Advances in Boundary Element Methods*, edited by C. Brebbia, Pentech, London, 1978, pp. 123-135.

[10] Banerjee, P. K., "Nonlinear Problems of Potential Flow," *Developments in Boundary Element Methods—1*, edited by P. K. Banerjee and R. Butterfield, Elsevier, London, 1979, pp. 21-30.

[11]Khader, M. S., and Hanna, M. C., "An Iterative Boundary Integral Numerical Solution for General Steady Heat Conduction Problems," *Journal of Heat Transfer, Transactions of ASME*, Vol. 103, No. 2, 1981, pp. 26-31.

[12]Onishi, K., and Kuroki, T., "On Nonlinear Heat Transfer Problems," *Developments in Boundary Element Methods—4*, edited by P. K. Banerjee and J. O. Watson, Elsevier, London, 1986, pp. 191-226.

[13]Wrobel, L. C., and Brebbia, C. A., "The Dual Reciprocity Boundary Element Formulation for Nonlinear Diffusion Problems," *Computer Methods in Applied Mechanics and Engineering*, Vol. 65, 1987, pp. 147-164.

[14]Wrobel, L. C., and Azevedo, J. P. S., "A Boundary Element Analysis of Nonlinear Heat Conduction," *Proceedings of the 4th International Conference on Numerical Methods in Thermal Problems*, edited by R. Lewis and K. Morgan, Pineridge, Swansea, Wales, UK, 1985.

[15]Azevendo, J. P. S., and Wrobel, L. C., "Nonlinear Heat Conduction in Composite Bodies: A Boundary Element Formulation," *International Journal for Numerical Methods in Engineering*, Vol. 26, No. 1, 1988, pp. 19-38.

[16]Kane, J. H., Wang, H., and Kumar, B. L. K., "Nonlinear Thermal Analysis with a Boundary Element Zone Condensation Technique," *Computational Mechanics*, Vol. 7, No. 2, 1990, pp. 107-122.

[17]Lachat, J. C., and Watson, J. O., "A Second Generation Boundary Integral Program for Three Dimensional Elastic Analysis," *Boundary Integral Equation Method: Computational Applications in Applied Mechanics*, Vol. 11, edited by T. A. Cruse and F. J. Rizzo, ASME, New York, 1975.

[18]Lachat, J. C., "Further Developments of the Boundary Integral Technique for Elasto-Statics," Ph.D. Dissertation, Southampton Univ., Southampton, England, UK, 1975.

[19]Lachet, J. C., and Watson, J. O., "Progress in the Use of Boundary Integral Equations, Illustrated by Examples," *Computer Methods in Applied Mechanics and Engineering*, Vol. 10, No. 3, 1977, pp. 273-289.

[20]Crotty, J. M., "A Block Equation Solver for Large Unsymmetric Matrices Arising in the Boundary Element Method," *International Journal for Numerical Methods in Engineering*, Vol. 18, No. 7, 1982, pp. 997-1017.

[21]Das, P. C., "A Disc Based Block Elimination Technique Used for the Solution of Non-Symmetrical Fully Populated Matrix Systems Encountered in the Boundary Element Method," *Proceedings of International Symposium on Recent Developments in Boundary Element Methods*, Springer-Verlag, Berlin, 1978, pp. 391-404.

[22]Bailecki, R., and Nahlik, R., "Linear Equations Solver for Large Block Matrices Arising in Boundary Element Methods," *Boundary Elements IX*, Vol. 1, Computational Mechanics Publications, Springer-Verlag, Berlin, 1987.

[23]Bailecki, R., "Nonlinear Equations Solver for Large Equation Sets Arising when Using BEM in Homogenous Regions of Nonlinear Material," *Boundary Elements IX*, Vol. 1, Computational Mechanics Publications, Springer-Verlag, Berlin, 1987.

[24]Tomlin, G. R., "Numerical Analysis of Continuum Problems in Zoned Anistropic Media," Ph.D. Dissertation, Southampton Univ., Southampton, England, UK, 1972.

[25]Butterfield, R., and Tomlin, G. R., "Integral Techniques for Solving Zoned Anistropic Continuum Problems," *Proceedings of the International Conference on Variational Methods in Engineering*, Southampton Univ. Press, Southampton, England, UK, 1971, pp. 9/13-51.

[26]Beer, G., "Implementation of Combined Boundary Element-Finite Element Analysis with Applications in Geomechanics," *Developments in Boundary Element Methods*, edited by P. K. Banerjee and J. O. Watson, Elsevier, London, 1986, Chap. 7.

[27]Mustoe, G. G. W., "A Combination of the Finite Element Method and Boundary Solution Procedures for Continuum Problems." Ph.D. Dissertation, Univ. of Wales, Univ. College, Swansea, Wales, UK, 1978.

[28]Davies, T. G., "Linear and Nonlinear Analysis of Pile Groups," Ph.D. Dissertation, Univ. of Wales, Univ. College, Cardiff, Wales, UK, 1979.

[29]Jin, H., Runesson, F., and Simuelsson, A., "Application of the Boundary Element Method to Contact Problems in Elasticity with a Nonclassical Friction Law," *Boundary Elements IX*, Computational Mechanics Publications, Springer-Verlag, Berlin, 1987, pp. 439-445.

[30]Margenov, S., Georgiev, K., Hadjikov, L., and Novakova, M., "An Effective Approach for Boundary Element Method Application to Friction Contact Problems," *Boundary Elements IX*, Vol. 1, Computational Mechanics Publications, Springer-Verlag, Berlin, 1987, pp. 439-445.

[31]Kane, J. H., "Shape Optimization Utilizing a Boundary Element Formulation," *BETECH 86, Proceedings 1986 Boundary Element Technology Conference, MIT*, Computational Mechanics Publications, Springer-Verlag, Berlin, 1986.

[32]Kane, J. H., and Saigal, S., "Design Sensitivity Analysis of Solids Using BEM," *Journal of Engineering Mechanics*, Vol. 114, No. 10, 1988, pp. 1703-1722.

[33]Saigal, S., and Kane, J. H., "A Boundary Element Shape Optimization System for Aircraft Components," *AIAA Journal*, Vol. 28, No. 7, 1990, pp. 1203-1204.

[34]Saigal, S., Kane, J. H., and Aithal, R., "Semi-Analytical Structural Sensitivity Formulation Using Boundary Elements," *AIAA Journal*, Vol. 27, No. 11, 1989, pp. 1615–1621.

[35]Saigal, S., Borggaard J. T., and Kane, J. H., "Boundary Element Implicit Differentiation Equations for Design Sensitivities of Axisymmetric Structures," *International Journal of Solids and Structures*, Vol. 25, No. 5, 1989, pp. 527–538.

[36]Kane, J. H., and Saigal, S., "Design Sensitivity Analysis of Boundary Element Substructures," *2nd NASA/U.S. Airforce Symposium on Recent Experiences in Multidisciplinary Analysis and Optimization*, Pt. 2, NASA CP 3031, 1988, p. 777.

[37]Kane, J. H., and Saigal, S., "An Arbitrary Condensing, Noncondensing Solution Strategy for Large Scale, Multi-Zone Boundary Element Analysis," *Computer Methods in Applied Mechanics and Engineering*, Vol. 79, No. 2, 1990, p. 219.

[38]Kane, J. H., and Saigal, S., "An Arbitrary Multi-Zone Condensation Technique for Boundary Element Design Sensitivity Analysis," *AIAA Journal*, Vol. 28, No. 7, 1990, pp. 1277–1284.

[39]Kane, J.H., Kumar, B. L. K., and Gallagher, R. H., "Boundary Element Iterative Reanalysis Techniques for Continuum Structures," *Journal of Engineering Mechanics*, Vol. 116, No. 10, 1990, pp. 2293–2309.